ISSN: 0974-5823 Vol. 7 No. 1 January, 2022

International Journal of Mechanical Engineering

Characterization of Nanostructured Structural Micro Crystalline (SMC) Al Alloys for Improved Mechanical Properties in Fractography

Kuwar Mausam, Rishabh Chaturvedi, Rajat Yadav

[1] Department of Mechanical Engineering, GLA University, Mathura

Abstract. The Nano structured Al alloys are becoming attractive due to its unusually high strengths. However, like all other nano materials they also exhibit low ductility which might restrict their uses in structural applications. A devitrified powder consolidated amorphous Al-Ni-Y-Co-Sc Alloy was subjected to another warm forging progression (673K, strain rate 10-1sec-1), which enhanced the post neck elongation by increasing the strain rate sensitivity (-0.02 at room temperature) The additional step of warm forging homogenizes the microstructure, globalizes the precipitates with high aspect ratios. These changes in morphology of the precipitates and the uniformity of microstructure achieved by the secondary forging process have brought about manifold improvement in total elongation%. However, the low strain hardening rate, which is the characteristics of nano structured materials, could not be improved and as a result the uniform elongation% remained low. The improved ductility of the secondary forged nano structured Al alloy has also been manifested in the fractography which shows dimpled type features with micro cavities.

Keywords: Nano, Ductility, SMC, Band, Dimples, Forging, Strain hardening.

1.1 Introduction

Please Nano Crystalline materials have found wide applications in MEMS, Bio, Magnetic, electronics and various other engineering fields[1-3]. The potentiality of very high strength of nano materials has made it attractive for structural applications also. For this purpose bulk processed structural nano materials have been studied by various investigators[4]. While SPD (severe plastic deformation) processing [5,6] e.g. ECAP (Equal Channel Angular Pressing), ARB (Accumulated Roll Bonding) etc. have been studied by the authors. On the other hand, PM routes of nano-powder consolidation have been investigated by others [6-8]. Most of the later investigators have described their work with devitrified amorphous glassy alloys. The processes have been dealt in detail by Akihisa Inoue in a review [9].found to reduce alarmingly [10-12] which is likely to restrict it's commercial applications. The low strain hardening rate could be due to the fact that it is impossible to retain dislocations inside a tiny grain as the grain boundary interactions are dominant and dislocation piling ups are very limited [13]. Wu et al have also observed similar behaviour in commercially pure nano structured Al alloy AA1050 [14-16]. Plastic instabilities occurred at a very early stage of deformation demonstrating very little uniform elongation. Shear band / Luder bands were observed in the beginning of tensile test[18-22]. Since it is seldom possible to extend the low uniform extension that is observed in nano grained materials, in this investigation, an attempt has been made to increase the post neck tensile elongation by delaying the fracture process[23-25]. In order to explore the possibility, an amorphous Al alloy (Al-Ni-Y-Co-Sc), devitrified by extrusion to Structurally Micro Crystalline (SMC) condition was chosen as initial stock which was subjected to secondary process of warm forging at various temperatures to modify the grain structure [26- 29].

2 EXPERIMENTAL

Structural Micro Crystalline (SMC) The “Al-4.0Ni-4.0Y-0.9Co-0.3Sc” (percentage point) alloy rods were produced by pressing the 'heat vacuum pressed gas atomized powders' at 673K (10:1 extrude) ratio. The finished rods were about 22 mm in diameter. The new specimens, obtained after extruding, would, here on words, be presented as (E).Cylindrical specimen objects of dimensions 22mmφ x 25 mm were isothermally set forged in a 2500 KN - MTS compression testing machine at three different temperatures 573, 598 and 623K with a strain rate of 10-1sec-1. Though 90 per cent of deformations were aimed at, the final sample dimensions were 55 mm x 4 mm thick due to the return. Most of the assessment work was carried out by pancakes formed at a temperature of 623K. Such forged + extruded specimens (623k, 10- 1sec-1) will be identified here on as (EF).Miniature tensile test pieces of gauge length 1.30 mm, width 1.08 mm and thickness 0.5 mm were tested from ‘extruded’ rods (E) and ‘extruded + forged’ pancakes (EF).

We test the test samples in a custom-built computer controlled 450 N tensile testing machine. The test was done by employing a strain rate of 2x10-4 sec-1, at various temperatures - RT, 473 K and 523 K. Three tests, at least, were done for every experiment and every situation of testing. For extruded rods (E) tensile tests have been done in transverse directions and longitudinal direction. In one test case , i.e. RT-2x10- 4 sec-1, the neck-corrected flow stress curve was also determined for (EF) sample by doing the trial three times to find the correct neck cross section.

In a compression testing machine of 100KN MTS, the compression test was performed at the same parameters (as the previous one). The miniature compressor test specimens were of size '4mm µx 4mm height.' Generally speaking, the ratio was lower by 1,5 in diameter to 1 when buckling facing high resistance and less ductile materials was avoided. It may take 5mmX5mm X5mm and 6mmX6mmX6mm rectangular samples for this purpose. BN was used for elevated temperatures while MoSi2 is used as lubricant at RT. However, the correction of friction was done with the 'friction factor (m)' in the present investigation. For these rings of "outside diameter (OD): inside diameter (ID): thickness (t)" In the 6:3:2-ratio the changes, the plotting for matching of the calibration curve, and the mathematical analysis of Avitzur with the machine algorithm, were compressed and 'm' was extracted from computations. From the given equation the frictionless, real stress curves were determined 18]:

$2m\ R$

$\sigma F\ = \sigma AP / (1 + 3\sqrt{3}\ H)$

Where σFC = Friction corrected stress, σAP=Apparently true tension, factor m=friction, radius R and cylinder height H. After making the above adjustment, the right curved of the friction and the true stress curve were shown in the figure. 1 for the terms of EF.

Normalised strain hardening rates "{ $\gamma = (1/\sigma)\ (d\sigma/d\varepsilon)$}" The tensile steps and the compression curves were measured at different points. These data are obtained through the creation of a computer programme that measures the stress and strain values numerically in any β standard. The strain hardening rates were determined from compression tests only because of very low and full elongations in tension of the extruded (E) specimens. Compression curves can only be determined for aIt has been noted that even though the tensile strength of nano materials increases substantially in all the bulk nano-structured materials, corresponding %elongation and relatively higher pressure, as no shift nor early failure occurs. A stress relief test and compression jump testing have been used to measure the Strain Rate Sensitivity Indices ('m').

Micro hardness test was done on primary samples i.e. Forged (EF) and extruded (E) parameters and on tensile and compression test samples at different steps of Deformation by using a 100gm load checking machine Buehler Micromet 5100 micro hardness. The fractured specimens were analyzed under scanning electron microscopes (SEM) of models JEOL - T330 and Hitachi - S4700 after testing of tensile and the localized band topology. The second one was used for splitting into two or more components of nano sized dispersoids. Transmission Electron Microscopic (TEM) analysis of thin specimens from extruded (E) and extruded + forged (EF) samples were taken to find the dimension and distribution of the parts and matrix. A 200KV Joel microscope of model JEM2000FX was used for this purpose.

3 RESULTS AND DISCUSSIONS

The bright field TEM image of (E) "Al-4.0Ni-4.0Y-0.9Co-0.3Sc" alloy sample, extruded as this, has been shown in Fig. 1. ~250 nm is the average size of matrix grain. The intemetallic particles that are generally in rod shapes with some also in spherical shapes are largely lying along the grain boundaries. 6o nm is an average diameter of the small spherical parts. The width and length of the particles of rod shape are 240 nm and 40 nm respectively.

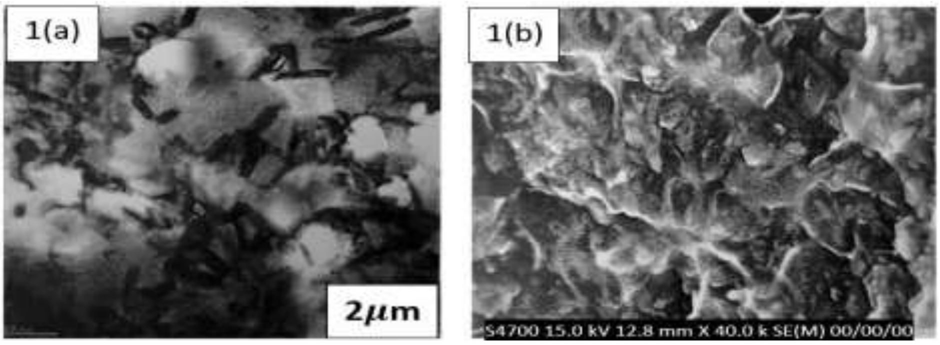

Fig. 1 (a) BF TEM image is of extruded (E) Al alloy presenting some round and some rod shape intermetallic dispersoids at the matrix grains boundary, (b) Fractography of tensile tested extruded sample

The results of longitudinal tensile test of extruded Al-4.0Ni-4.0Y-0.9Co-0.3Sc alloy rods (E) checked at normal temperature have been presented in table 1, which shows low ductility in terms of total extension percentage. Variations between samples are large whereas the 0.2% PS and UTS are extremely high, which might be greatly attributed to the unequal distribution of different dispersoids. Most of the transverse specimens fractured early before coming the yielding point; ductility was nil. Since the particles were closely settled and gathered near boundaries of the grain as shown in Fig. 1 (a), the tensile extruded object could have cracked early, rather than nuclear micro-voids, which could have formed atomic bonds on grain boundaries some amount of ductility by delaying the fracture process.

Table 1. Mean tensile characteristics of Extruded (E) samples at "RT, 2 X10-4 s-1"

Samples	0.2 % P.S., MPa	UTS, MPa	%El
Extruded Transverse	633 56	667 57	1.1 1.5
Extruded Longitudinal	661 ±41	664 ±41	2.1 0.4

Study of fractography from the broken tensile samples as illustrated in Fig. 1 (b) demonstrates shallow dimples with less defined shear lips and very few micro voids, indicating the brittle nature of fracture which is largely responsible for premature failures of as extruded (E) samples.

The tensile strengths after forging the extruded (E) rods at different temperatures (573k, 598k and 623k) have been compared in Fig.2(a) which demonstrate that forging at the higher temperature of 350°C (623k) could be better for ambient temperature strength and also for elevated temperature of 250°C (523k). Importantly, the total elongation% at ambient temperature is also higher for the sample forged at 350°C (623k) as illustrated in Fig.2 (b). The total elongation% contains both uniform and post neck elongations. The scatter in elongation% is noticeable at all temperatures, which could be attributed to the non uniform distribution of precipitate particles. The observation of ductility minimum is often observed in metals and alloys [19,20]. The ductility minimum temperature (DMT) was described as an unexplained feature. The present one occurring at 200°C (473K) in this alloy has not been dealt in this investigation.

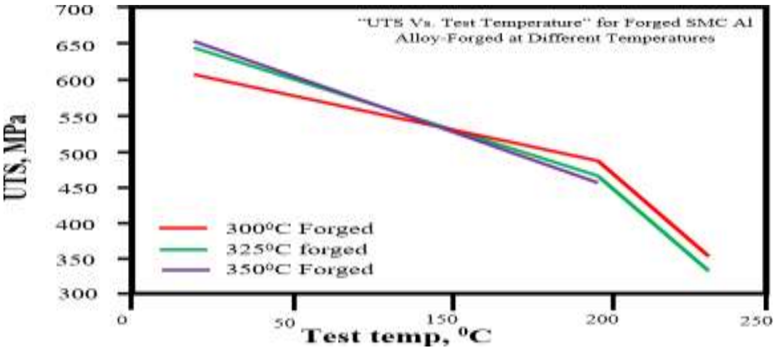

Fig.2 Comparison of (a)UTS

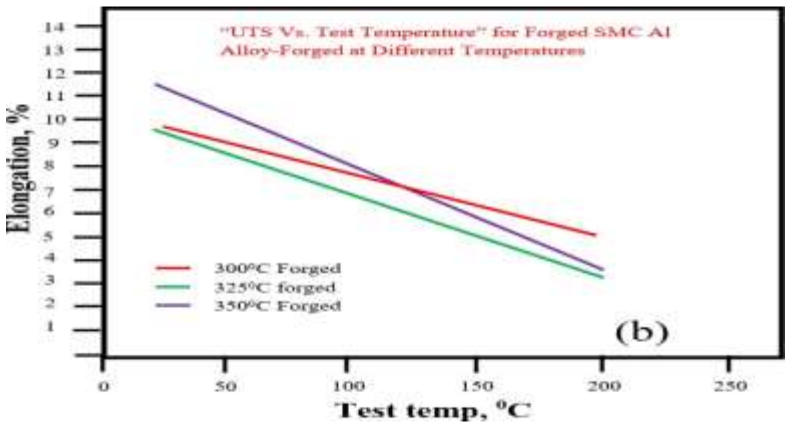

Fig. 3 Elongation%, after forging of the extruded rods at 300°C (573k), 325°C (598k), 350°C (623k).

Rather, in the present investigation we shall restrict our discussions to the observations made at the maximum forging condition of 623K, 10-1sec-1 only, which is presented as (EF). While the tensile strengths in 'as extruded' and 'extruded + forged' conditions didn't vary significantly as illustrated in Fig.4 (a), the total elongation% after forging improved noticeably to 11.5% as shown in Fig.4 (b). The mean elongation% of as extruded sample was 1.1% only. The wide scatter of elongation% is an indication of uneven distribution of the intermetallic precipitates.

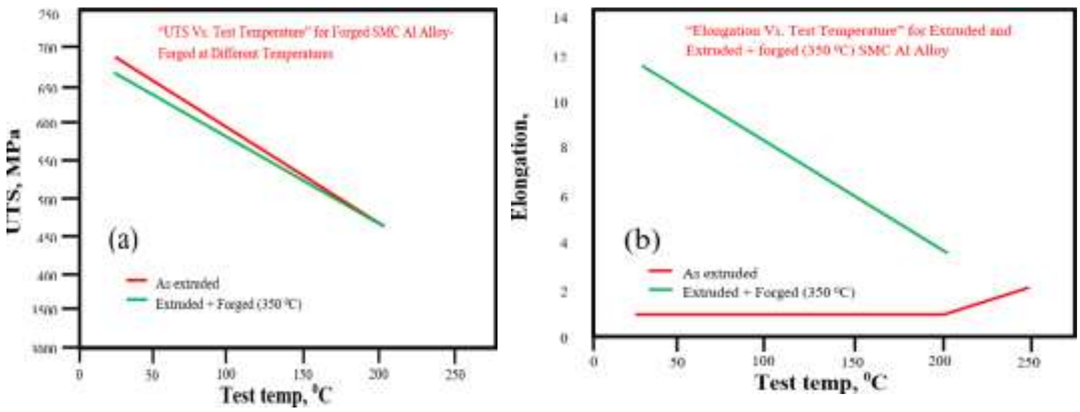

Fig.4 Comparison of (a) UTS and (b) Elongation% of 'as extruded' and 'extruded + forged 350 0 C (623k)

It can however be noted that the uniform elongation% are low for both 'extruded' and 'extruded + forged' samples. which is obviously because of the lower strain hardening rates for both 'extruded' as well as 'extruded + forged' conditions as shown in the table 2.

*γ [=(1/σ).(dσ/dε)] for extruded samples were calculated from compression test. During the very beginning of After the load limit, which is sustained until the failure, the tensile test can be found immediately after the tensile band neck, but deformation persists within dispersed neck borders. It has been shown [18, 21] that the instability for diffused neck is guided by Hart's criterion i.e. (γ + m < 1) while that for band neck it is, "where γ = Normalised Strain hardening rate = (1/σ).(dσ/dε), and m = strain rate sensitivity index". It could be noticed from table3 that instabilities due to strain hardening rate (γ) sets in at very low strain values, both for diffused as well as localized band neck. During the tensile test it is noticed that although the localized neck of the band has been present the deformation starts almost from the start of the neck elongation stage up to a certain strain in the reshaped neck. The test target, however, eventually breaks in the region of the band (localized neck).

Table 2. Tension and compression tests standardized strains harding (α) for various varieties obtained.

γ = (1/ σ).(dσ/dε)*	Strain		Remark
	Compression	Tension	
1	0.022	0.015	γ >1- uncertainty for diffused neck
½	0.028	0.018	γ >1- uncertainty for localized neck
0	0.040	0.035	Softening starts
-0.23	0.70	-	High softening rate

From this observation it may be hypothesized that at the primary stage of the creation of the neck, The strain rate increases locally, producing the stress rate hardened in the field, according to the equation ̈= k as soon as the deformation starts to place in the neck of the band. This can only be achieved if the stress rate index is fairly high 'm', as in case of extruded + forged condition (m =

-0.028), vide table4. The reshaping, thus, moves to the comparatively softer area i.e., It continues and also hardens in the diffused neck. Finally, deformation occurs again in the band region leading to the break-down of the test component, as it is likely to dilute rapidly due to the current pressure of the plane.

Table 3. Strain rate sensitivity index (m), determined for Extruded (E) and Extruded + Forged (EF).

Test temperature	Strain rate sensitivity (m)	
	Extrude (E)	Extruded + Forged (EF)
RT	0.003	0.02 (0.028 from stress relaxation)

In order to obtain this postulation that we have calculated micro hardness on the tensile piece at different stages of deformations (strains).039). The hardness variables were shown graphically in the Figure in different stages of tensile testing (and compression). As requested, the hardness value for the localised band neck (184.3 HV point (a at 4 percent tensile strain (β = 0.039) was relative high and for other areas of the diffuse neck, at another 154.9 HV (b) was lower. Clearly, because of flow-sufficiency in this process of pressure, the diffused region of the nck is smoother compared to the main forged (172,3 HV. point a). As shown in table 3, strain relaxation should be applied ε = 0.024. The rise of hardness in the localized band neck has happened because of higher strain rate hardening (as dictated by higher m-value of 0.02). As the strain increased to 14%, the

band neck hardness came down to 160.3 (point c) and the tensile sample fractured. Fig 5. Shows the variations of hardness in extruded + forged tensile sample at different stages of strains 0 % strain, (b, b') 4% strain, (c)14% strain, (d) 45% strain, (e) as extruded, 0% strain.

~

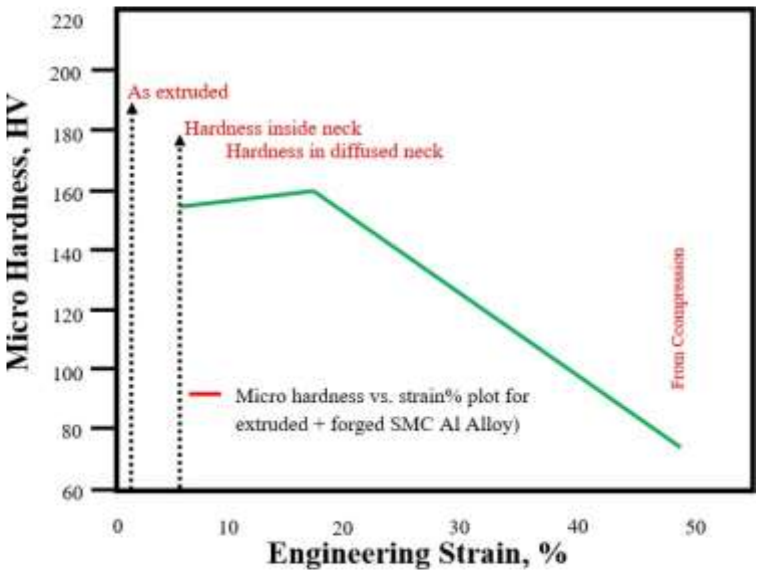

Fig 5. Variations of hardness in extruded + forged tensile sample at different stages of strains -

0% strain, (b, b') 4% strain, (c)14% strain, (d) 45% strain, (e) as extruded, 0% strain

Point d in Fig.5 has been taken from compression test sample, as 45% deformation is not achievable in tensile deformation. The hardness drops to 76.2 HV only, due to a huge softening rate γ = - 0.23, vide table3.

After forging the extruded sample, the particles shows an unsystematic spreading. The tensile fracture face of the extruded + forged (EF) sample seems to present laminary types of breaks which may have produced along the planal preliminary particle boundaries. The high initial aspect of the particulate matter (~6) was loosened to 2-3 (PPB). That turned out to be aligned dimples closely (or micro voids). Many bolts have one or two particles that mean that the particle matrix interfaces have been initiated by the micro voids. On the other hand, the surface of the broken extrude specimen as shown in Fig.1(b), does not demonstrate that the dimples grow or align as a function.

4 CONCLUSIONS

- A very high tensile elongation (~11%) can be obtained in "Al-Ni-Y-Co-Sc" alloy, introduce a secondary forgery process (623k – 10-1 sec-1) after extrusion.
- The high tensile elongation is possible because of the development of relatively high 'm value (~0.02), accomplished after the second process of warm forging
- The results of investigations show that SMC structure obtained in titanium and its alloys by severe plastic deformation is characterized by the presence of high elastic stresses and elevated density of dislocation in grains.
- Refinement of grains to submicron sizes leads to a decrease in the material density, some increase in the elastic modulus while a value of the damping factor remains the same.
- The main hot forging reduces the homogenized distribution of the intermetallic particles and the appearance ratio.
- The unique work to failure in bending for the SMC alloy is three times that of the alloy in the MC annealed condition. This behavior results in lower resistance to crack formation as well as crack growth.

References

1. Author, Y.M. Wang, E. Ma, Three strategies to achieve uniform tensile deformation in a nanostructured metal, Acta Mater., 52, 2004, pp1699-1709.
2. Goyal, M., Shape, size and phonon scattering effect on the thermal conductivity of nanostructures. Pramana, 2018. 91(6): p. 87.
3. Sharma, K., K.S. Kaushalyayan, and M. Shukla, Pull-out simulations of interfacial properties of amine functionalized multi-walled carbon nanotube epoxy composites. Computational Materials Science, 2015. 99: p. 232-241.
4. C.Y. Yu, P.W. Kao, C.P. Chang, Transition of tensile deformation behaviors in ultrafine- grained aluminum, Acta Mater., 53, 2005, pp 4019-4028.
5. Goyal, M. and B. Gupta, Study of shape, size and temperature-dependent elastic properties of nanomaterials. Modern Physics Letters B, 2019. 33(26): p. 1950310.

6. R. S. Mishra, R. Z. Valiev, S. X. McFadeen, R. K. Islamgaliev and A. K. Mukherjee, High strain-rate superplasticity from nanocrystalline Al alloy 1420 at low temperatures, Phil. Mag. A, 81, no. 1, 2001, pp 37-48.
7. Yadav, A., et al., Glass transition temperature of functionalized graphene epoxy composites using molecular dynamics simulation. Integrated Ferroelectrics, 2018. 186(1): p. 106-114.
8. C. Suryanarayana, The structure and properties of nanocrystalline materials: issues and concerns, JOM, vol.54, no.9, Sept. 2002, pp 24-27.
9. Akihisa Inoue, Amorphous, nanocrystalline and nanocrystalline alloys in Al-based system, Progress in Materials Science, 43, 1998), pp 365-520.
10. A.L. Vasilev, M Aindow, M. J. Blackburn, T. J. Watson, Phase stability and microstructure in devitrified Al rich Al-Y-Ni alloys, Intermetallics, 12, 2004, pp 349 – 362.
11. Singh, P.K., et al., Effects of functionalization on the mechanical properties of multiwalled carbon nanotubes: A molecular dynamics approach. Journal of Composite Materials, 2017. 51(5): p. 671-680.
12. W. J. Golumbfskie, M. F. Amateau, T. J. Eden, J. G. Wang, Z. K. Lieu, Structure property relationship of a spray formed Al-Y-Ni-Co Alloy, Acta Materialia, 51, 2003, pp 5199- 5209.
13. X. L. Shi, R. S. Mishra, T. J. Watson, Elevated temperature deformation behaviour of nanostructured Al-Ni-Gd-Fe alloys, Scripta Materialia, 52, 2005, pp 887 – 891.
14. Y. Wang, X. L. Shi, R. S. Mishra and T. J. Watson, Ductility improvement in devitrified ultrafine-grained Al-4.0Y-4.0Ni-0.9Co alloy via hot rolling, Scripta Materialia, 56, 2007, pp 923 925.
15. Kumar, A., K. Sharma, and A.R. Dixit, A review of the mechanical and thermal properties of graphene and its hybrid polymer nanocomposites for F.: Article title. Journal 2(5), 99–110 (2016
16. structural applications. Journal of materials science, 2019. 54(8): p. 5992-6026.
17. H. Miyamoto, K. Ota, T. Mimaki, Viscous nature deformation of ultrafine grain aluminum processed by equal channel angular pressing, Scripta Materialia, 54, 2006, pp1721-1725.
18. B. Q. Han, Z. Lee, D. Witkin, S. Nutt and E. J. Lavernia, Deformation behaviour of bimodal nanosructural 5083 Al alloys, Metallurgical and Materials Transactions, vol. 36A, April, 2005, pp 957-965.
19. Kumar, A., K. Sharma, and A.R. Dixit, Carbon nanotube-and graphene-reinforced multiphase polymeric composites: review on their properties and applications. Journal of Materials Science, 2020: p. 1-43.
20. S. X. Li and G. R. Cui, Dependence of strength, elongation and toughness on grain size in metallic materials. Journal of Applied Physics, 101, 2007, pp 0835251-0835256.
21. S. Hariprasad, S. M. L. Sastry and K. L. Jerina, Deformation behaviour of a rapidly solidified fine grained Al-8.5%Fe-1.2%V-1.7%Si alloy, Acta Materialia. vol.44, no. 1, 1996, pp 383-389.
22. Youssef K. M., Scattergood R.O., Murty K. L., Horton J. A., Kotch C. C., Applied Physics Letter. 87 (9). 2005, 091904.
23. T. Male and V. Depierre, The validity of mathematical solutions for determining friction from the ring compression test, J. Lubr. Technol. (Trans. ASME), vol.92, 1970, pp 389- 397.
24. Shukla, M.K. and K. Sharma, Improvement in mechanical and thermal properties of epoxy hybrid composites by functionalized graphene and carbon-nanotubes. Materials Research Express, 2019. 6(12): p. 125323.
25. G.Saul, A. T. Male and V. Depierre, A new method for determination of material flow stress values under metalworking conditions, Technical report AFML-TR-70-19, U.S. Air Force Materials Laboratory. Jan., 1970.
26. Edward M. Mielnik, Metalworking Science and Engineering. McGraw-Hill Inc,NW, 1991.
27. Kumar, K., et al., Experimental Investigation of Graphene-Paraffin Wax Nanocomposites for Thermal Energy Storage. Materials Today: Proceedings, 2019. 18: p. 5158-5163.
28. M. A. Arkoosh and N. F. Fiore, Elevated Temperature Ductility minimum in Hastelloy alloy X, Metallurgical and Materials Transactions B. vol.3, no.8.1972. pp 2235-2240.
29. R. Nowosielski, P. Sakeiewicz, P. Gramatyka, The effect of ductility minimum temperature in CuNi25 alloy, Journal of Materials Processing and Technology, 162-163. 2005. pp 379- 384.
30. Dutta, P.S. De, R. S. Mishra and T.J. Watson. Deformtion Behaviour of an Ultrafine Grained Al-Ni-Y-CO-Sc Alloy. Materials Science & Engineering A. vol.513-514, 2009. pp 239 -